

Development and Testing of a Contra-Rotating Marine Current Turbine on a Flexible Mooring

Joe Clarke, Gary Connor, Andrew Grant, Cameron Johnstone
Energy Systems Research Unit
Department of Mechanical Engineering
University of Strathclyde
Glasgow, Scotland
Email: esru@strath.ac.uk

Introduction

This report describes the development and testing of a Contra-Rotating Marine Current Turbine (CoRMaT) against a concept established by the Energy Systems Research Unit at the University of Strathclyde. The system, comprising turbine and submersible contra-rotating generator is neutrally-buoyant allowing it to be connected to a flexible, tensioned mooring (Figure 1). The project, which was undertaken over several years with support from EC/UK Research Councils and Scottish Enterprise's Proof of Concept scheme, involved modelling to inform design decisions, tow-tank testing to resolve operational issues, and sea trials to confirm performance under real operating conditions.

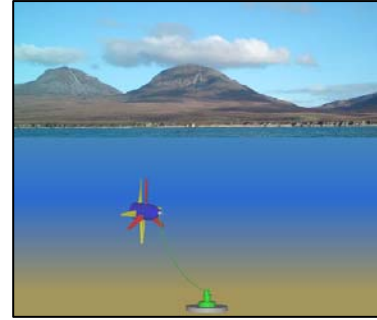


Figure 1: CoRMaT deployed.

The core feature of CoRMaT is its two rotors arranged in close proximity around a common axis of rotation [1, 2]. This arrangement minimises the reactive torque transmitted to the supporting structure, permitting the use of a relatively simple mooring system and allowing deployment in deep water. While the early stages of marine current exploitation are likely to be served by turbines on fixed piles [3] or gravity bases, there is significant advantage to be obtained from deploying machines in deeper water using flexible, tensioned moorings. CoRMaT may therefore be regarded as a next generation design whose operation hinges on the idea of 'flying' a neutrally-buoyant turbine from a single-point mooring. The issues relating to stability and station-keeping in streams with variable speed and direction were addressed within the project.

A second feature of CoRMaT follows from the reactive torque minimisation: the reduction of wake swirl allowing greater turbines packing density for a given site. It is widely accepted [4] that wake-turbine interaction may prove to be a major limiting factor in the exploitation of coastal sites. There is evidence from studies on helicopter rotors [5] that contra-rotation produces a fundamentally different wake structure, with more favourable dissipation characteristics and this attribute has been optimised within the CoRMaT design [6].

The project was executed in several stages: initial modelling studies to inform preliminary design decisions, tow-tank tests to confirm performance and optimise design parameters, and sea trials to test complete systems at realistic scale.

Initial design

The blade element theory [7] technique was initially applied to a conventional, single-rotor turbine to equate forces on the blade and on the fluid stream:

$$dF = 4\pi r \rho V_\infty^2 a(1-a)dr = \pi \rho \sigma W [C_L \Omega r(1+a') + C_D V_\infty(1-a)]r.dr$$

for the axial, stream-wise component, and

$$dS = 4\pi r^2 \rho V_\infty (1-a)a'\Omega.dr = \rho W \sigma [C_L V_\infty(1-a) - C_D \Omega r(1+a')]r.dr$$

for the tangential component.

These equations were solved by an iterative process to produce converged values of the flow parameters a and a' , after which the velocity vectors shown in Figure 2 were evaluated. Performance

predictions for the complete rotor were obtained from a summation over all blade elements after making an appropriate allowance for blade tip losses.

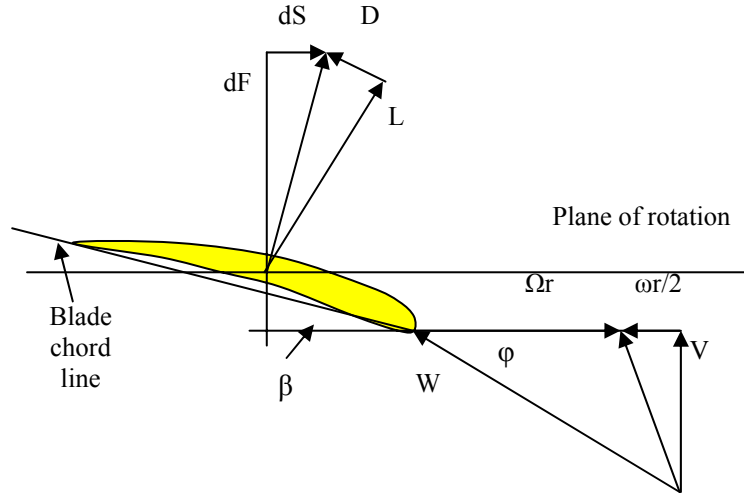


Figure 2: Vector diagram for up-stream rotor.

To predict the performance of the two contra-rotating rotors, certain assumptions were made. First, it was assumed that the rotors are in close proximity and function as a single actuator disc as far as blade element theory is concerned. Second, it was assumed that the swirl imparted to the flow by the upstream rotor is removed by the rotor downstream, i.e. there is zero reaction torque transferred to the structure which supports the rotor pair (this characteristic would later be confirmed by experiment). The procedure adopted was to prescribe a geometry for the upstream rotor, obtain converged solutions for a and a' , and use these to specify an appropriate geometry for the downstream rotor.

To obtain a closed solution to the momentum equation for the upstream rotor, a further assumption is required. It is clear that the equation above for dF is no longer correct: the upstream rotor will only experience a fraction of the total retarding force on the fluid stream, and it is necessary to specify this fraction for the equation to be solved. In practice, a wide range of conditions may occur, and these would need to be investigated. But also in practice, a rotor would be designed for optimum performance in certain specified flow conditions.

A symmetrical case was used where the rotors run at the same tip speed ratio and it was assumed that each experiences the same axial thrust loading, equal to one half of that experienced by the fluid stream. Therefore:

$$\lambda_1 = \lambda_2, \quad dF_1 = dF_2, \quad \text{and} \quad dS_1 = dS_2$$

where subscripts 1 and 2 refer to upstream and downstream rotors respectively. Extending this to each blade element, the equation for dF (for the upstream rotor) is modified to

$$dF = 2\pi r \rho V_\infty^2 a(1-a)dr = \pi \rho \sigma W [C_L \Omega r (1+a') + C_D V_\infty (1-a)]r.dr.$$

The equations were then solved to give values of a and a' . For the rotor as a whole, parameters such as axial thrust, torque and power output were computed at this stage. For the downstream rotor, the velocity and force vector diagrams (Figure 3) are similar, but not identical, to those upstream. The flow angle ϕ is obtained from

$$\tan \phi = \frac{V_\infty (1-a)}{\Omega r}$$

so ϕ is known if a has been determined. The momentum equations reduce to

$$\frac{\sigma C_N}{2} = \frac{a}{1-a} \sin^2 \phi \quad \text{and} \quad \frac{\sigma C_T}{4} = a' \sin \phi \cos \phi$$

where $C_N = C_L \cos \varphi + C_D \sin \varphi$ is the axial or normal thrust coefficient, and $C_T = C_L \sin \varphi - C_D \cos \varphi$ is the tangential force coefficient. These may be combined to eliminate σ :

$$\frac{C_T}{C_N} \tan \varphi = \frac{2a'(1-a)}{a}.$$

This equation is solved by iteration: values of the blade pitch angle β are presented until a solution is found. Solidity σ is then calculated, and the blade chord length determined. Blade tip losses were again included using the method of Prandtl. Whether this is appropriate for the downstream rotor is, at this stage, uncertain in the absence of experimental data.

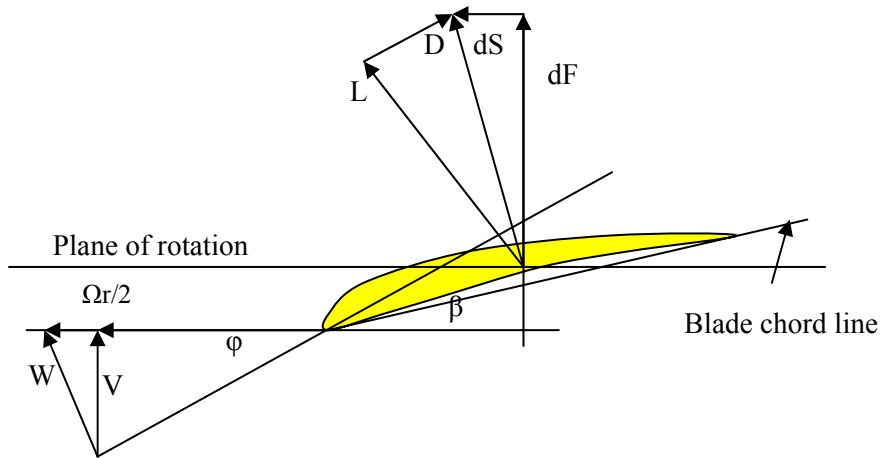


Figure 3: Vector diagram for down-stream rotor.

The method was used to predict turbine geometry and performance for a number of different upstream rotor configurations. Specifications for this rotor were drawn up using established procedures [7], setting the blade pitch distribution for high efficiency at the design point but choosing chord lengths which were larger than those which gave optimal power coefficient. The aim was to produce a robust rotor while retaining acceptably high performance. The aerofoil section used for both rotors was NREL S814 [8], which performs well at moderate Reynolds Numbers and is relatively insensitive to surface imperfections, an important consideration when a small model is to be tested. The simplest turbine configuration consistent with good dynamic behaviour was chosen, with 3 blades upstream and 4 downstream. All computational models used a diameter of 0.82 m, the size selected for towing tank tests. At the specified design point, the tip speed ratio for each rotor was 3.

Figure 4 shows the chord and pitch distributions finally selected for the test model. Distributions of blade chord length and pitch angle (beta) show similar but not identical trends for the two rotors. Some numerical instability was observed in calculations near the tip for the second rotor, apparently due to the effects of tip losses. In this region, values of chord and pitch extrapolated from trends further inboard were used in the production specifications. The predicted power coefficient for the turbine at its design point was 0.3846.

A second computational code, again based on blade element theory, was then used to predict the performance of this model turbine for a range of operating conditions. Inputs to the code consisted of blade geometries for the two rotors, the stream velocity and the tip speed ratio for each rotor. Blade chord and pitch distributions predicted by the original design code were extracted as polynomial equations, to be used as data input for these subsequent calculations (and later for CNC machining of the blades themselves). As before, it was assumed that the torques on the two rotors should be equal, giving zero net reaction torque. However, axial thrust loadings need not be equal when running off-design. At first, an attempt was made to replicate the design condition of $\lambda_1 = \lambda_2 = 3$. As with the

previous code, it was necessary to specify the ratio of axial thrust loadings for the rotors at the outset. The code would then predict the torque and thrust for each rotor.

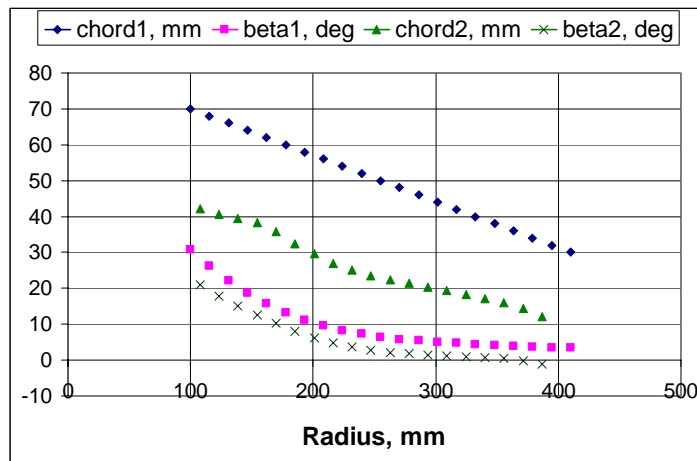


Figure 4: Design blade chord and pitch distributions for the contra-rotating turbine model.

For the design condition, of course the values for each rotor should be the same. For off-design conditions (say $\lambda_1 = 4$), the procedure was to input values of λ_2 and axial thrust ratio, and iterate until a solution was found in which the torques were equal and the axial thrust ratio equalled the specified value. The outcome was a series of operating points for selected values of λ_1 . The results obtained were encouraging. For zero net reaction torque at $\lambda_1 = 3$, the precise conditions required were $\lambda_2 = 2.875$, with an axial thrust distribution of 51% and 49% for the upstream and downstream rotors respectively. This contrasts with the 50%/50% axial thrust distribution and $\lambda_2 = 3$ specified in the original design. Given that blade chord and pitch data were not identical to the outputs from the design code (having been smoothed for ease of manufacture), some small discrepancies would be expected. Full characteristics were then determined for the turbine: i.e. for C_P and λ ($= \lambda_1 + \lambda_2$).

The performance prediction code permitted investigation of the effect of changing blade pitch angle (a facility which was not included in the final design). Figure 5 shows a comparison of C_P/λ characteristics as a function of increasing the pitch angles (on both rotors) by 2° and 4° . It is apparent that the nominal blade angle settings for this design do not maximise the value of C_P and a small increase in pitch angle is desirable. Peak values above 0.4 are then attainable. Even at the nominal blade angle setting, maximum C_P is not reached at the design tip speed ratio of 6, but higher.

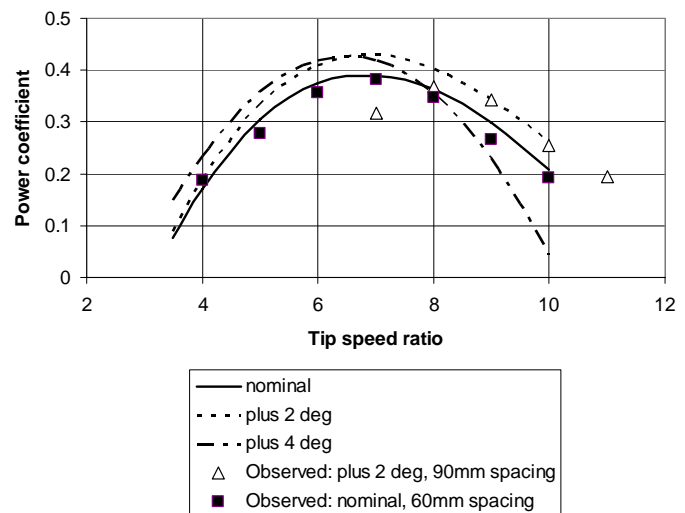


Figure 5: Effects of blade pitch angle on rotor performance.

The relative performance of conventional and contra-rotating machines has been illustrated by simulating a single-rotor turbine with the same geometry as rotor 1

(see Figure 3). Predicted values of power and axial thrust coefficients are shown in Figures 6 and 7; for the contra-rotating turbine, where the tip speed ratio is $\lambda_1 + \lambda_2$. In theory, a contra-rotating machine is capable of higher power coefficients by eliminating the swirling velocity component in the wake, but this is generally small and, as seen here, the peak values of C_P are similar. The contra-rotating turbine works best at high tip speed ratios as expected: its peak thrust coefficient is some 15% higher

than for the single-rotor turbine, but of course in the example given here its overall solidity is nearly twice as great.

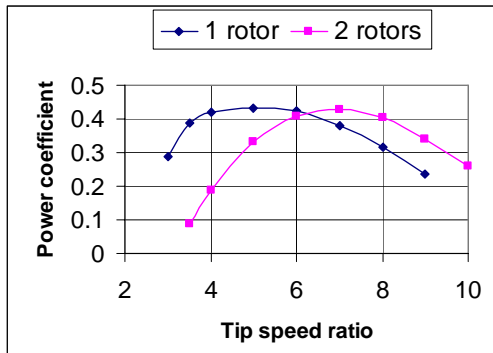


Figure 6: Predicted power coefficients for conventional and contra-rotating turbines.

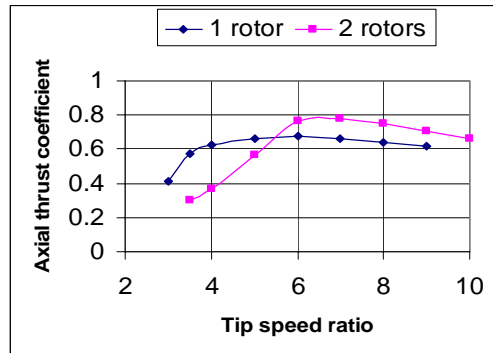


Figure 7: Predicted axial thrust coefficients for conventional and contra-rotating turbines.

Tow-tank tests

A prototype turbine was constructed for tow-tank testing, with blades cut from T6082 aluminium alloy on a CNC milling machine, using patterns derived from the computational design process. Split hubs clamped the blade roots while allowing infinite variation of pitch angle. The two co-axial stainless steel rotor shafts ran underwater in plain polymer bearings without lubrication. A CAD schematic of the submerged drive train is shown in Figure 8. The CNC process left shallow grooves on the blade surfaces, running in the chord-wise direction. Blade profiles were slightly under-cut to allow for subsequent powder coating, which increased blade thickness and greatly reduced the depth of the grooves, to less than 0.2 mm throughout. Final blade profiles were accurate to within ± 0.5 mm.

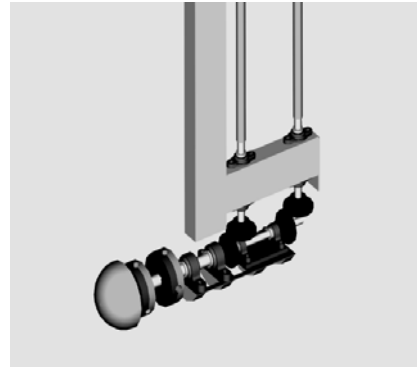


Figure 8: CAD rendering showing drive train detail.

It was considered impractical to fit a submerged generator to such a small model, so loading was applied by mechanical friction. To meet the condition of zero net torque, the same brake load had to be applied to each rotor; however, it was important that the rotors were free to turn at different speeds. A differential gearbox was constructed to meet these criteria and frictional load was applied by a small disc brake, hydraulically actuated. Brake and gearbox were located above the water surface, drive from the rotors travelling via bevel gear sets and vertical semi-rigid drive-shafts. The co-axial rotor shafts were housed in a cylindrical shroud, attached to a vertical beam, which in turn was clamped to the carriage of the towing tank. The complete assembly, raised out of the water for inspection, is shown in Figure 9. When testing, the submerged section of the beam was fitted with a streamlined fairing to reduce pressure build-up and drag. The overall diameter of each rotor was 0.82 m. Axial spacing between the rotors was adjustable, from 45 mm (the practical minimum) to 100 mm.



Figure 9: The test rig raised out of the tank and on the carriage.

Instrumentation

Optical encoders were placed on the drive-shafts from each rotor above the water-line, where they entered the differential gearbox, to record shaft speeds. Strain gauge bridges recorded bending

moments in a number of locations: on the main supporting strut to measure thrust loading; on the arm which held the disc brake calliper to indicate braking force and hence frictional torque; and at the root of one blade on each rotor. On the blades, two full bridges were positioned to record in-plane and normal bending moments. All data sampling and processing was performed by LabView software. Static calibrations before and after testing verified the robustness of the sensor systems, repeatability being within 1%.

Transfer of strain gauge data from the two contra-rotating rotors posed some problems. Initially each rotor hub contained a compact data storage device in the form of a WAV format recorder; however, the timing synchronisation of records for accurate dynamic analysis of blade/blade interactions was insufficiently reliable. The final solution adopted employed the multiplexing of high frequency electrical signals from the 4 strain gauge channels (normal and edgewise on each rotor) via slip-rings to a single LabView input channel. Data de-multiplexing was carried out in software to reproduce the strain-gauge data sampled at 1300 Hz, equating to a rotor angular resolution smaller than 1° .

Test procedure

The tests were carried out at a single depth of immersion and a fixed carriage speed of 0.8 m/s, which was found to be sufficient for stable running. The Reynolds Number based on rotor diameter was about 6.5×10^5 . Runs were made with increasing brake loads until one or both rotors stalled. Several rotor axial spacings and blade pitch angles were investigated.

Power Coefficient

The mechanical drive train of the test turbine imposed a significant resistive torque even in the absence of any applied friction at the disc brake. A comparison of torques calculated from in-plane blade bending moments and from the load on the brake calliper arm indicated a discrepancy of about 11% even at maximum power. A substantial discrepancy would therefore be expected throughout the range, so blade root bending moments were used to calculate shaft torque and hence power output. Experimental values of power coefficient were plotted against tip speed ratio as superimposed points in Figure 5. The maximum turbine power output in all tests at 0.8 m/s towing speed was directly measured as 127 W, corresponding to a peak C_p of 0.39 at a tip speed ratio of about 7.

At nominal blade pitch angle, the agreement with predictions of power coefficient is remarkably good. For pitch angles 2 degrees above nominal, excellent agreement is again seen at high tip speed ratios, but significant discrepancies are apparent elsewhere. This latter series of tests was carried out with a larger inter-rotor spacing, and the downstream rotor tended to stall under heavy loads. The minimum stable tip speed ratio was limited to 7, and performance at slightly higher ratios seemed to be adversely affected. Also of course, wide spacing between rotors departs from the ‘single actuator disc’ assumption implicit in the blade element theory of the computational model. Examination of other test data series should clarify the issue.

No allowances have been made for blockage effects in the towing tank. Water depth during testing was 2.3 m, with the rotor axis at mid-depth. The overall blockage was about 5% of the cross-section, based on the swept area of the turbine and the submerged frontal area of the supporting strut.

Dynamic effects

Time series recordings from the strain gauge bridges are presented in Figure 10. These indicate blade root bending moments in the plane of rotation, and normal to this plane, for one blade in each rotor. In the captions, R1 refers to the upstream 3-bladed rotor, R2 to the 4-bladed rotor downstream. A period of 2.75 s is displayed, covering more than 2 complete revolutions for each rotor. This particular record was obtained with the turbine running close to its maximum power coefficient, with a tip speed ratio of 7.25.

From both predictions and experimental observations, it is clear that blade bending loads are very large for marine current turbines. In a real operating environment (as distinct from a towing tank), dynamic loading from velocity shear, rotor misalignment and water-borne turbulence must be

considered. For rotors near the surface, waves may add a significant cyclic load [9]. Finally, blade/strut interaction will create a once-per-revolution perturbation.

In a contra-rotating turbine, further cyclic loads from blade/blade interaction would be expected. For the turbine tested, with 3 and 4 blades, disturbances might occur at frequencies of $4(f_1 + f_2)$ for the upstream rotor and $3(f_1 + f_2)$ for the downstream one, where f_1 and f_2 are the rotational frequencies of the upstream and downstream rotors respectively.

Some general conclusions were drawn from the results of Figure 10. The case presented here is a particularly disturbed one, with the two rotors in close proximity and with rotor 2 close to the vertical supporting strut. Normal (stream-wise) loads for rotor 1 are reasonably steady, as expected. Also as expected, data for rotor 2 show more variation, with perturbations in some places coming at a frequency consistent with blade/blade interaction.

Edge moments (in the plane of rotation) for rotor 1 are again fairly steady, with a small-amplitude ripple at frequency f_1 caused by gravity. Signals for rotor 2 show much larger excursions, and are still under investigation. The lengthy, gear-driven power take-off system of the test model may be a factor here. The large number of “spikes” in the edge moments for both rotors may have the same cause. In the example presented, it appears that there is a significant discrepancy between the two mean blade bending moments in the plane of rotation. Allowing for the fact that there are 4 blades on rotor 2 and only 3 on rotor 1 a discrepancy in mean shaft torques is still apparent, if the data are valid. Friction in the drive train was substantial for this small model, and if unequally distributed would provide an obvious explanation. The assumption of equal torques ($dS_1 = dS_2$) made in the performance predictions may therefore not have been borne out in practice, at least in this (fairly extreme) case.

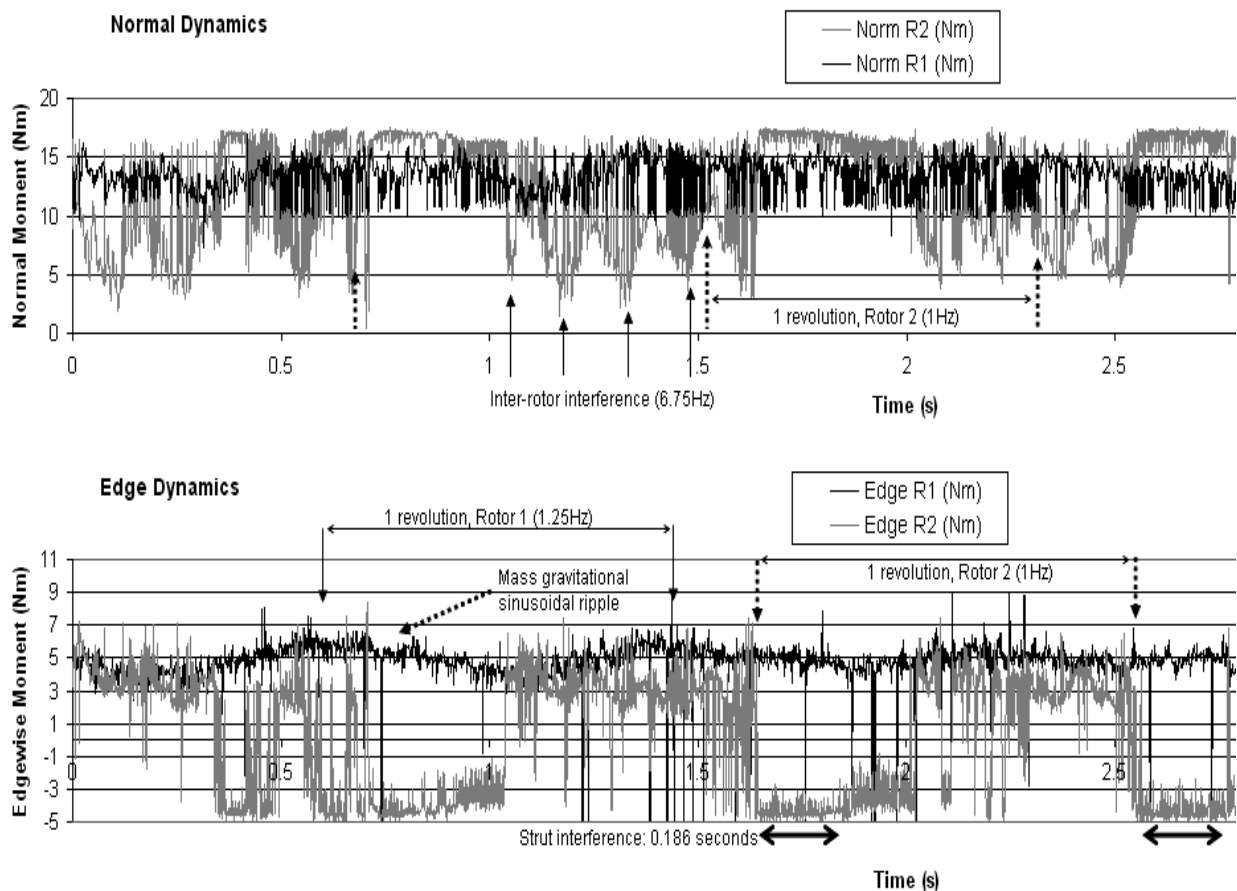


Figure 10: Blade root bending moments in two planes, rotor 2 in proximity to main strut.

Sea trials

On the basis of the results of the tow-tank tests, a 2.5 m diameter turbine was constructed as shown in 1. Sea trials in the Clyde Estuary confirmed the inherent stability of the design and provided high-resolution measurements of blade bending moments, from strain gauges attached to blade roots on both rotors. Of particular interest was the loading on the downstream blades, as the turbine configuration inevitably raises questions about blade/blade interactions and consequent fatigue loading.



Figure 11: CoRMaT deployed in the Clyde Estuary.

Figure 12 gives time-series data for the turbine during normal operation, with both rotors turning at similar (but not identical) speeds. Because the upstream rotor has 3 blades, blade/blade interaction in the turbine would be expected to manifest itself as pulses at a frequency of $3(f_1+f_2)$, where f_1 and f_2 are the rotational frequencies of the individual rotors. There is no clear evidence of this, either from direct observation or from a study of corresponding Fast Fourier Transforms (FFT) of the data series as shown in Figure 13. Lower-frequency perturbations are present, from gravity and interaction with parts of the supporting framework. In the figure, P refers to multiples of the rear rotor rotational frequency.

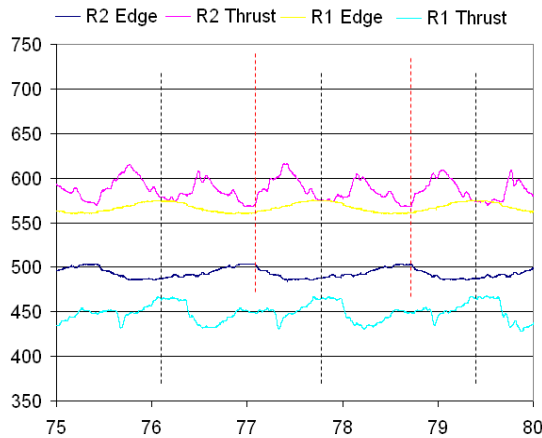


Figure 12: Blade bending moment data for upstream (R1) and downstream (R2) rotors.

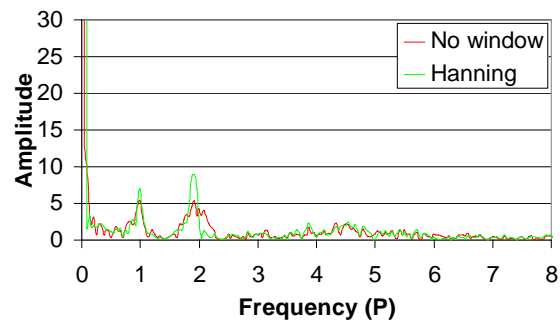


Figure 13: FFT for rear blade thrust loading during normal operation.

In contrast, a time series was obtained when the upstream rotor was deliberately stalled. The experimental data given in Figure 14 shows large regular shock loadings on the downstream blade as it passes through the bluff body wake created by the stationary blades upstream.

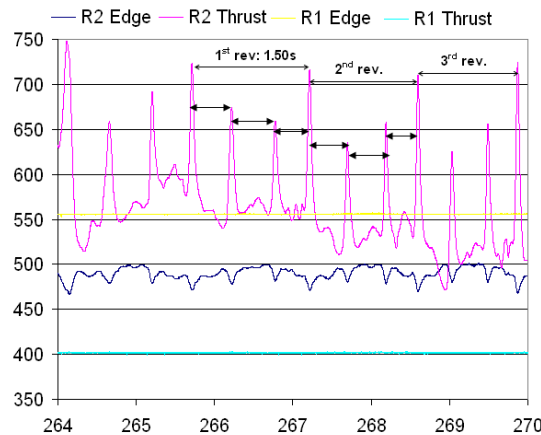


Figure 14: Time-series blade bending moment data for upstream (R1) and downstream (R2) rotors (arbitrary scale, R1 stalled).

Taken together, Figures 12 and 14 give insight into the magnitude of the cyclic loads experienced during normal turbine operation. The spectrum is dominated by gravitational loads and the wakes behind fixtures, which can be minimised by design. Blade/blade interactions are relatively small.

Mooring

CoRMaT is designed to operate from a tensioned mooring secured to the sea-bed. To prove the feasibility of the concept, a mooring system was designed and tested. One problem is to provide sufficient buoyancy to maintain the operating depth of the turbine between reasonable limits; even at small scales this is not easy to accomplish. The solution was to employ an auxiliary float as shown in Figure 15.

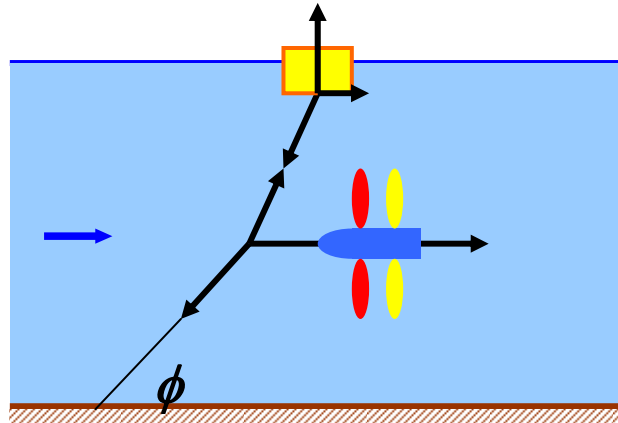


Figure 15: A neutrally-buoyant turbine on a tensioned cable.

Here the turbine itself has near-neutral buoyancy with the residual provided by the tensioning float. For the lower part of the cable, static analysis simplifies to the equation

$$\tan \phi = \frac{F_D}{B}$$

where B is the buoyancy force and F_D the summation of the drag forces on the turbine and float; the latter may be substantial and can be significantly reduced by placing the float on the surface in cases where wave excitation is not problematic.

The intention with this configuration would be to operate at small values of ϕ by building in greater excess buoyancy. Variations in operating depth with current velocity V would then be significantly reduced. The effects of scale may have an influence on the choice of mooring configuration. Drag forces rise approximately with the square of the linear dimension, whereas buoyancy increases with the cube. Figure 16 illustrates the required spherical surface float or floatation chamber size as a function of turbine rating.

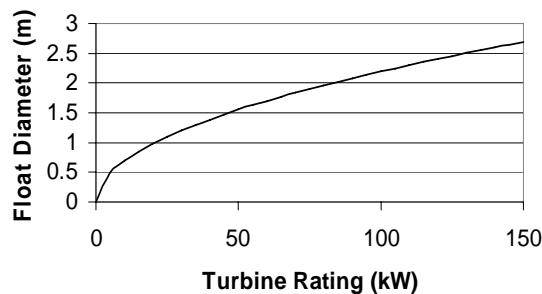


Figure 16: Float diameter versus turbine rating (maximum tidal velocity = 2.5 m/s).

The active material weight of the Permanent Magnet Generator (PMG) is likely to be the most significant part-mass of the turbine. The PMG mass may be calculated by rearranging the following equation:

$$P = 4\pi^2 J.r_i B.n.a(r_o^2 - r_i^2)$$

where J is the conductor maximum current density, r_i the inner core radius, r_o the outer core radius, B the average flux density in the winding, n the rotational speed, and a the winding axial thickness. In this equation r_o was set to be $\sqrt[3]{3} r_i$ thus optimising the power for a given outside diameter and loading [7]. This is unlikely to be an optimal mechanical or economic design, but allows sufficient radius information to estimate the weight of a PMG. This was added to the calculation for buoyancy used to produce Figure 16.

There are a number of issues pertaining to the use of these moorings for marine current turbines which require further investigation. One is the behaviour at slack water, where the turbine must avoid fouling the mooring, and re-align itself when the current starts to flow. A number of solutions are possible including motoring a main rotor or the use of modified marine thrusters to provide yaw control.

Another issue is cable twist: the repeated uni-directional circular motions of the device about its tethering point would eventually damage the electrical power cable, which must necessarily follow the route of the main cable to the sea bed. The aforementioned yaw mechanism could provide an unwind function, or a slip-ring style electrical coupling could be employed – the life-cycle duty of such a mechanism being very small compared to that used in high-speed machinery.

Yet another issue is stability in turbulent flows: tests on small models in flumes indicated that the shape of the nacelle may be an important factor. With some shapes, oscillations in yaw or pitch seem to occur despite the large self-aligning effect of the drag force on the rotor itself.

Complete system prototype

This prototype was designed to allow examination of the following operational features:

- the performance of the complete contra-rotating power train;
- the production of electricity from a submerged generator; and
- the stability of the complete system when deployed on a single-point mooring.

The turbine employs a direct-drive generator, resulting in a large nacelle diameter. There was also a demand for a reasonably high rotational speed, which imposed limits on overall rotor diameter. The result was a turbine with hub diameter 0.43 m and overall diameter 0.92 m. The complete turbine is illustrated as a cut-away drawing in Figure 17.

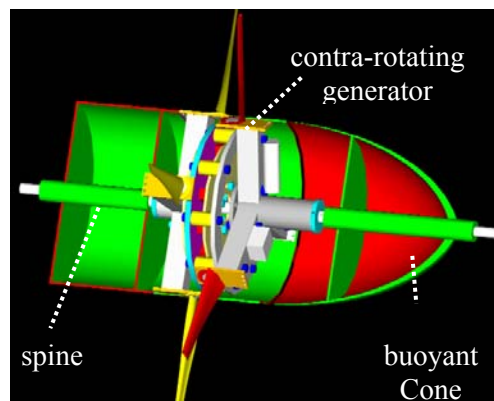


Figure 17: CoRMAT components.

Despite the bulky nacelle, it was found to be difficult at this scale to go much beyond neutral buoyancy, and a tensioned cable with auxiliary float (Figure 15) was adopted for the trials. While it has been recommended that the generator diameter should not be greater than 10% of the rotor diameter for wind turbines [7], it is presently unknown whether this holds for tidal machines. Two options exist to reduce the diameter of the generator:

- several axial generator units may be connected in series on the same frame; or

- the electrical output may be generated at a lower frequency and converted to the frequency required (although core copper losses increase significantly at very low frequencies [10]).

Direct drive generator

The relatively slow rotational speed of a tidal turbine necessitates a gearbox to increase the speed suitably for a common four-pole generator. Another option is a direct drive generator with a large number of poles. The advantage of this approach is the higher overall power take off efficiency – typically 90% near the rated load [11] compared to around 85% for a costly multi-stage high torque gearbox (4-stage efficiency of 94%) and generator (90%) combination [12]. Other advantages include greater reliability and reduced maintenance requirement.

The direct drive generator constructed for CoRMaT has an axial magnetic field created by 24 Neodymium-Iron-Boron (Nd-Fe-B) N50 grade permanent magnets distributed on the 2 rotors making up 12 magnetic poles, and sandwiching the stator, which contains 9 copper windings encased within a polymer resin disk. Nd-Fe-B magnets have vastly superior magnetic properties over traditional Ferrite magnets. The flux density B_r of the chosen magnets is 1.42T. The maximum operating temperature (150°C) of Nd-Fe-B magnets is unlikely to be an issue in a submerged tidal generator.

The axial-flux generator is configured to provide a 3-phase electrical output. This is converted to DC via a 3-phase rectifier. The energy may therefore be efficiently transmitted underwater and inverted at the grid end, or (in this experimental case) fed into a resistive dumped load by a Pulse Width Modulated (PWM) driven Insulated Gate Bipolar Transistor (IGBT), allowing the turbine microcontroller to regulate the overall turbine speed and attain maximum C_p throughout the tidal cycle. The contra-rotating prime mover torque balance critical to maintaining the zero reactive torque, and thus providing turbine hydrodynamic stability, is provided inherently by the magnetic flux linkage across the stator-rotor air gap. The generator is depicted in Figures 18 and 19.



Figure 18: Encapsulated coils and permanent magnets of the contra-rotating axial flux generator.



Figure 19: Generator location within the turbine nacelle.

The generator is submersible so that both the rotors and stator operate in sea water. Although the magnetic properties of sea water and air are not significantly different, the electrical insulating properties and corrosive abilities certainly are. The rotors and nickel coated permanent magnets are therefore coated in a hard wearing polymer to provide corrosion protection. The stator is constructed from polyurethane resin into which the copper coils are hermetically sealed with glands allowing the electrical output cables to exit the generator. The advantages of a generator open to sea water are:

- ease of construction;
- generator/nacelle casing leaks are tolerable;
- cooling is provided naturally;
- there are no complex sealing requirements; and
- there is no large diameter seal friction.

Possible drawbacks include:

- lowered efficiency due to the hydro-dynamic effects of rotating parts; and
- marine growth on exposed components.

The first drawback is partly mitigated by the relatively low rotational speeds and the hydro-dynamically efficient design of the exposed parts. Marine growth will be mitigated by the high levels of water turbulence experienced within the generator, the speed of rotation, the use of anti-fouling compounds and/or the installation of a mechanical ‘wiper’ system on active generator surfaces.

Sea trial test results

Figure 20 shows the prototype as deployed for sea testing. The electrical load was contained in a pod attached below the surface buoy to provide natural sea water cooling. The pod also contained power electronics (smoothing and PWM), a single 8 channel Gigalog stand-alone data recorder with 1GB data card, and a microprocessor to provide data processing and control functionality. Instrumentation, power and communications cables accessed the pod through IP68 cable glands backed up by a polyurethane resin back-fill. The sensors aboard the turbine included: Rotor1_RPM, Rotor2_RPM, Inclination_Roll, Inclination_Pitch and Velocity_tide. while the sensors encapsulated within the pod included: PMG_Voltage, PMG_Current, Buoy_Roll and Buoy_Pitch. The microprocessor monitored the same data as the solid state recorder but turned it into an RS232 stream, which was sent to both the data recorder and via the surface buoy antenna as telemetry to the support vessel. Buoy inclinometer channel, M_y , is the synchronising data stream between the 2 Gigaloggers, the second of which is on top of the buoy and described later.

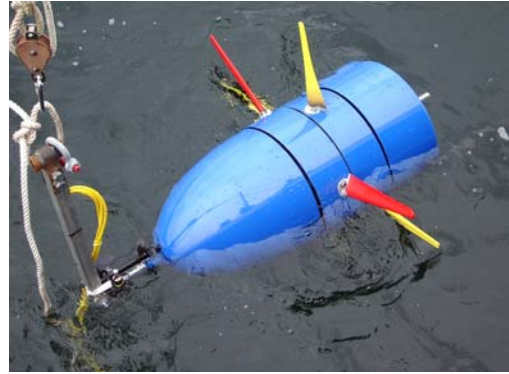


Figure 20: CoRMaT sea trial.

The microprocessor used to provide data acquisition, RS232 radio communications and turbine control was a Microchip PIC 16F877. This was chosen due to its multi-channel, 10bit ADC, RS232 communication capability, hardware PWM module, and robust low-cost low-power architecture. The device was programmed using a MELabs PIC Programmer and the MELabs PICBasic Integrated Development Environment. The PICBasic code is included in the filestore, as are the circuit diagrams and PCB layouts for the controllers. A bi-directional RS232 (from microprocessor) to Bluetooth converter and radio link was purchased and configured to provide the wireless data stream back to a laptop PC on the support vessel. This was found to work well at distances of up to 250 m between the support vessel and turbine.

The surface buoy had a strut through it, at the upper end of which (out of wave action) was attached two IP56 boxes containing batteries to power the instrumentation, a second Gigalog data recorder, strain gauge amplifiers for the 2 load cells (mooring and turbine connection), and the radio communications device/antenna. A GPS logger was included to assist with tidal flow recording. The NMEA files are contained in the test files.

Kyles of Bute test results

The St Hilda was used to undertake an initial tow-test to tune the operation of the system, particularly the control and data acquisition components. Battery duration was tested and extrapolated to check the time available in standalone mode before recovery was required. Data was measured at 10 Hz and each of the system components was tested thoroughly. The mooring load-cell data and turbine data channels were synchronised to allow later comparison of results.

Experimental results are shown in Figure 21. The generator output voltage indicates the duration of the towing period. The turbine nacelle is fitted with inclinometers to monitor its attitude in the flowing stream. Measurements indicated excursions in pitch and roll up to 15° from nominal, possibly in response to turbulence downstream from a rather heavy towing strut. But the stability of such a bulky device (hub diameter almost 50% of the overall diameter) is likely to be poor; the more elegant proportions of larger, production turbines should confer more sedate behaviour.

It is emphasised that a good peak hydrodynamic efficiency is not essential to achieving the aims of the test programme. Performance of the turbine was compromised to some extent by the decision to use existing blades, whose chord and pitch distributions had originally been optimised to suit a different set of parameters. Predictions of power and thrust coefficients (C_P and C_t) for the complete 2-rotor machine are given in Figure 22. The tip speed ratio at which peak C_P is achieved reflects the geometric limitations imposed on the design; a higher value would perhaps have been desirable.

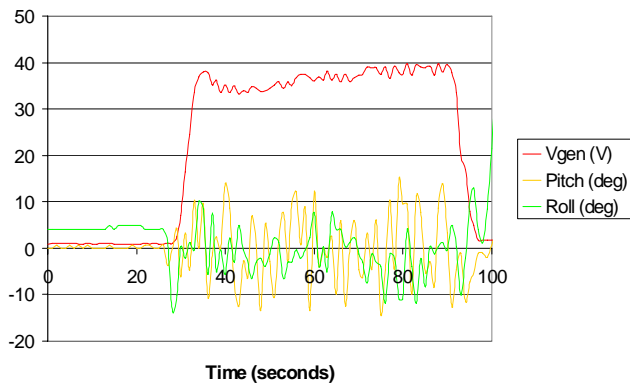


Figure 21: Pitch and roll results from sea trials.

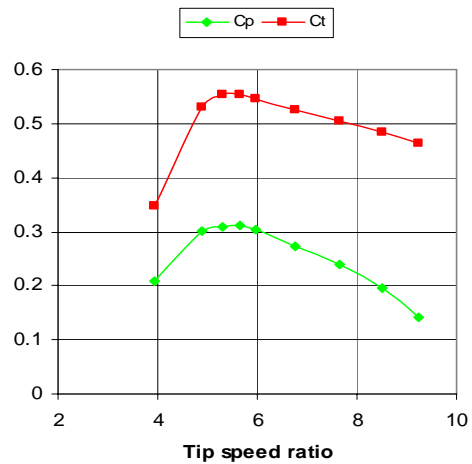


Figure 22: Turbine performance in sea trials.

It can be observed from Figures 23 and 24 that power was generated (a peak of approximately 45 W at 0.8 m/s, equating to a C_p of 0.21), although as the device was allowed to run at a high load resistance the voltage often drifted beyond the 64 V maximum of the monitoring equipment. This was noted as a lesson for the later Islay tests in addition to a higher sampling frequency (100 Hz) being necessary to properly capture the digital pulses of the 2 tachometers measuring rotor rpm. The pitching is noted to vary quickly with a total range of 30° with obvious results on the power quality. Additionally, some roll is present although in gradually varying amounts probably brought on by the constantly changing boat direction through an arc (to prevent collision of blades with St Hilda's hull).

The load cells show 2 trends: a very periodic loading pattern at a frequency of around 2.5 Hz and a much slower varying loading distribution. The slower changes in loading are associated with the interactions with the St Hilda – when the turbine is on deck, being deployed, or being manipulated to avoid collision with the side of the vessel. While these results confirmed the correct functioning of the load-cells, they provided no useful data for turbine analysis purposes.

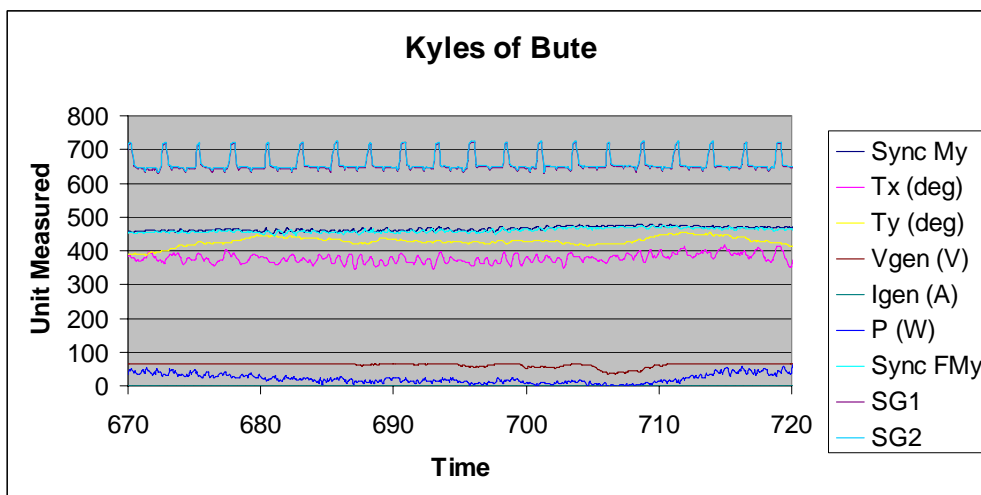


Figure 23: Kyles of Bute test data (MCADC OP2).

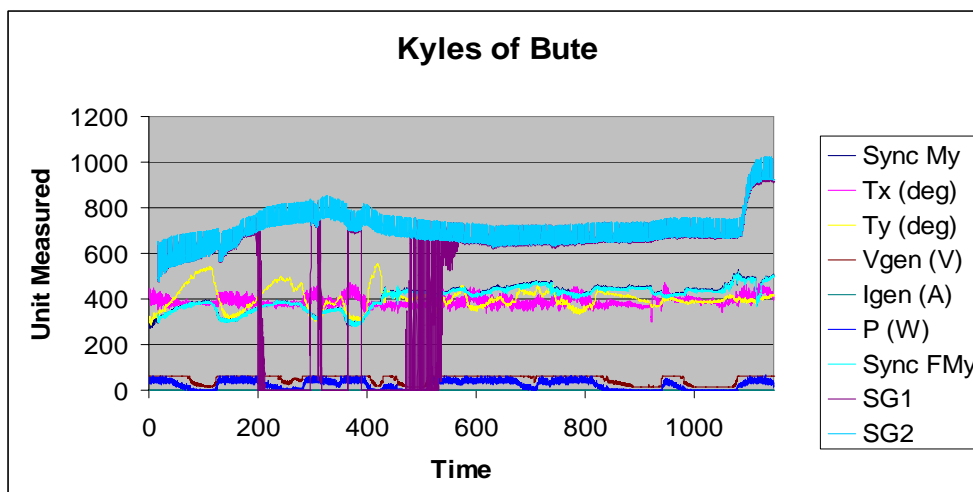


Figure 24: Kyles of Bute test data (MCADC OP2).

Sound of Islay test results

Following on from the Kyles of Bute trails, CoRMaT was deployed in the Sound of Islay in two locations as shown in Figure 25 and data recorded for the aforementioned channels at 100 Hz.

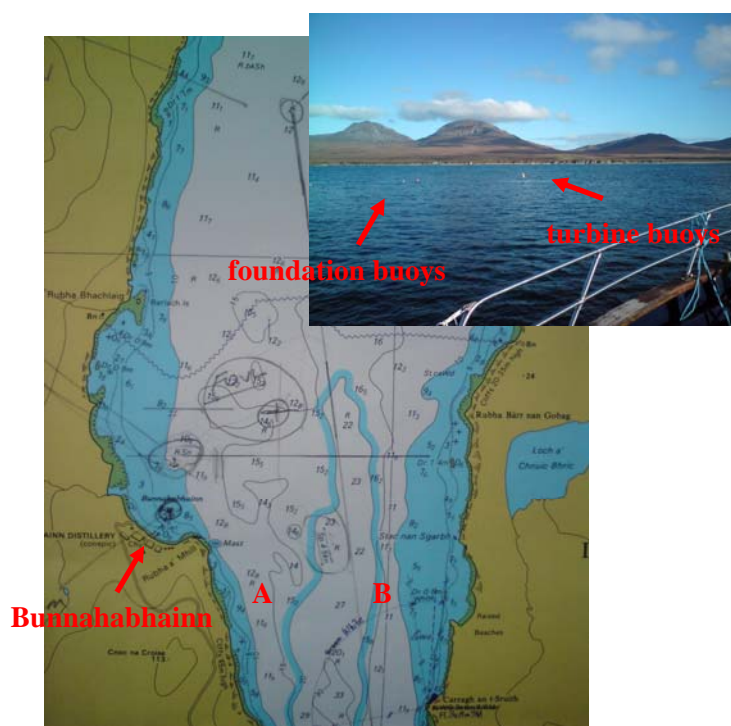


Figure 25: Sound of Islay test sites - inset photo is of site B.

Figure 26 gives sample results from deployment at 16 m at location B (initial deployment at location A experienced a gradual decline in power output as eddies formed and the tidal flow diminished). It is notable that the voltage varies considerably over very short periods of time. This is most likely to do with turbine instability (turbulence, shear, dynamics etc) producing varying rotor yaw angles, hence rotor rotational fluctuations which feed through to the power train and directly to voltage output. It is clear that the power (negative due to current direction and to more clearly show the synchronicity with voltage) varies in line with voltage fluctuation. The only outlier to this is the small power spike when the load on the turbine is increased using the PWM load control. The tidal speed measured also varies with yaw, although the output is seen to vary from just below 0.5 m/s to 0.67 m/s. When equated to

power output (using a moving average to partially remove yawing fluctuations), this produces C_p values of between 0.21 and 0.28.

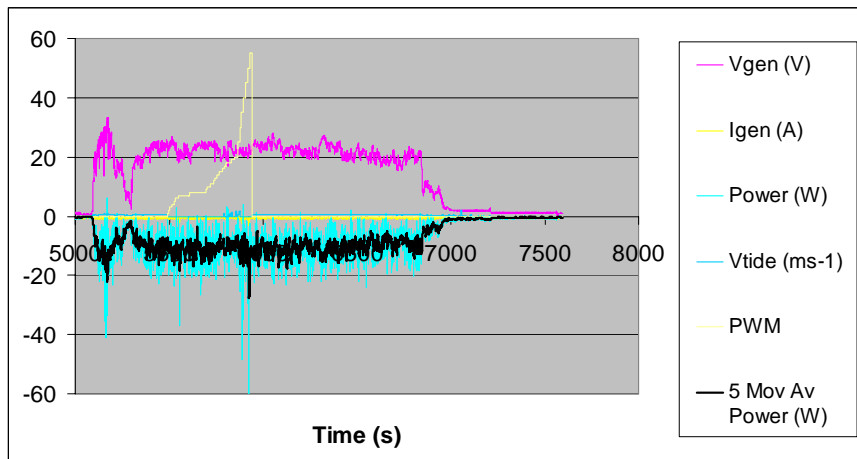


Figure 26: Operational data from CoRMaT testing.

High speed inclinometer data was recorded as illustrated in Figure 27 and mapped by Fast Fourier Transform (FFT) to allow determination of the dominant modes of pitching and rolling frequencies.

Figure 28 shows the dominant pitching frequencies during a 30 minute period of testing in the Sound of Islay tidal stream. As expected, some small rotor dynamic frequencies are observed (F_1 and F_2) due to slight blade misalignments in the test rig set-up. However, frequencies F_n and F_3 are of an amplitude that would require system modification. F_n is the dynamic instability present due to the non-ideal size of the nacelle. It is possible to use a proportionally smaller nacelle as the device is scaled up and this mode would then disappear. F_3 was found to be due to vortex shedding behind the vertical tubular section connecting the turbine to the surface buoy, which would not be present in a scaled-up deployment as the buoy would not be necessary.

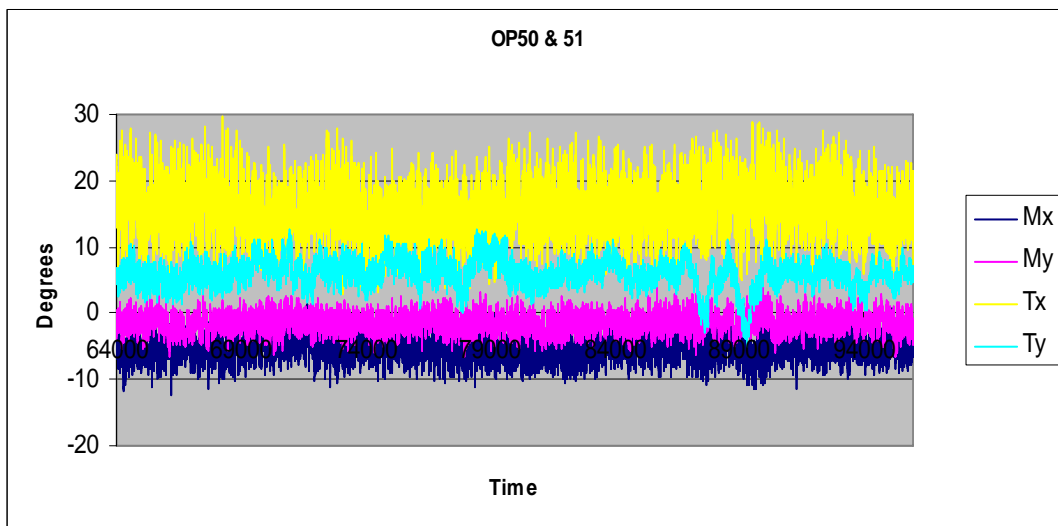
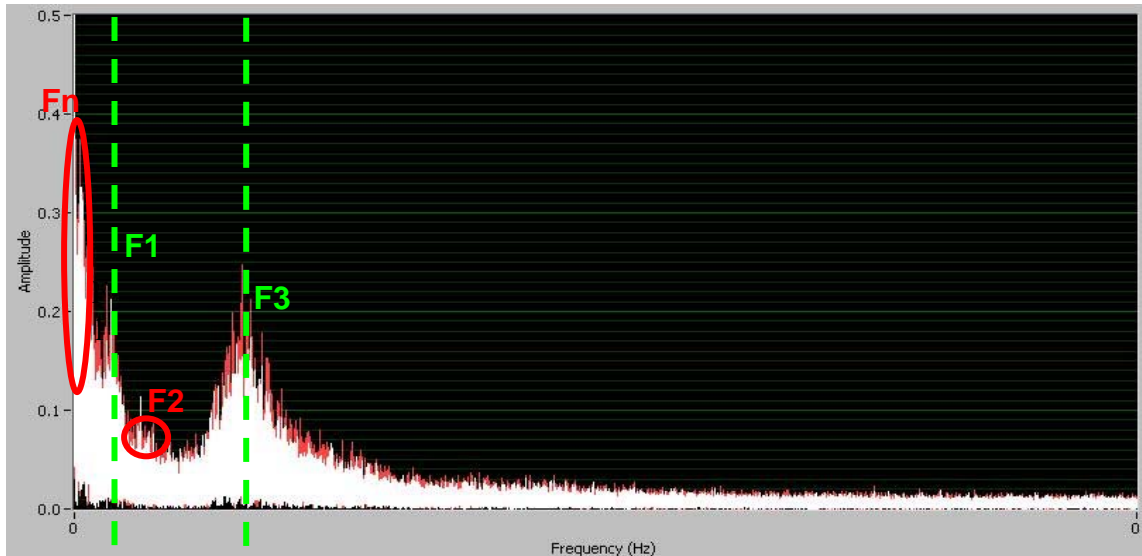


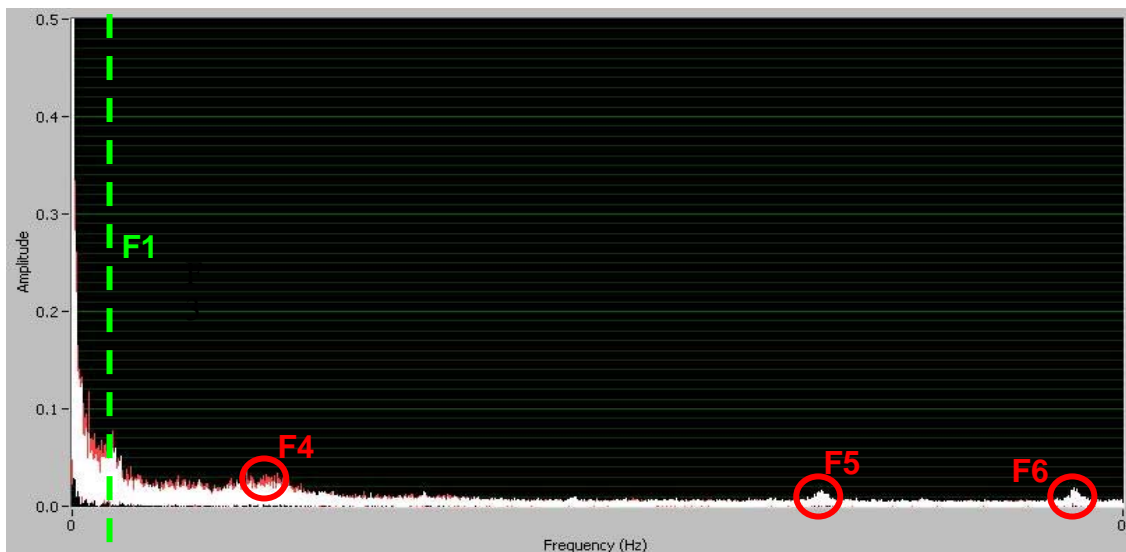
Figure 27: Real-time CoRMaT pitch and roll data.

Figure 29 shows the dominant roll frequencies during the same 30 minute period of testing. F_1 is again observed, while it is the non-uniform layout of the axial flux generator that produces the very small frequencies of F_5 and F_6 . These can be negated by careful PMG build as would be expected during full-scale industrial manufacture using bespoke jigs.



| Pitch | F_n | F_1 | F_2 | F_3 |
|-------------------|-------------------|---------------------------|----------------------------|--|
| Freq. (Hz) | 0.597 | 1.792 | 3.885 | 8.167 |
| RPM | 35.85 | 107.56 | 233.13 | 490.03 |
| Source of dynamic | Oversized nacelle | Fundamental rotor 1 speed | Total combined rotor speed | Karman vortex shedding from buoy strut |

Figure 28: FFTs of CoRMaT pitch data showing the dominant frequencies.



| Roll | F_1 | F_4 | F_5 | F_6 |
|-------------------|---------------------------|-----------|---|---|
| Freq (Hz) | 1.859 | 9.362 | 35.657 | 47.742 |
| Rpm | 111.55 | 561.75 | 2139.44 | 2864.54 |
| Source of dynamic | Fundamental rotor 1 speed | $5 * F_1$ | PMG stator non uniformities ($9 * F_2$) | PMG magnet non uniformities and blade-blade interactions ($12 * F_2$) |

Figure 29: FFTs showing the dominant CoRMaT roll frequencies.

Wake studies

Wake development is an area where it is expected that contra-rotation will prove uniquely beneficial: the absence of a coherent, swirling component because the blade/blade interactions bring about rapid mixing and wake dispersion. To investigate the issue small model turbines (250 mm diameter) were placed individually or in arrays in an open, 1 m wide flume. Each turbine was connected to a DC motor via a step-up gearbox; the motor functions as a generator, allowing rotational speed to be

controlled by varying the external electrical load. In an array of turbines, wake interference will result in a diminution in power output: monitoring this allows the effects to be quantified. Supporting evidence was provided by velocity traverses, carried out by a 3-component ultrasonic probe at various locations upstream and downstream of the turbines and arrays.

As shown in Figure 30, with a single turbine, the wake showed no sign of dispersion immediately downstream. Instead, the wake extends quickly beyond the swept area of the rotor but then stabilises, with subsequent slow velocity recovery (except in the region immediately behind the turbine hub). This finding concurs with earlier work using mesh discs to represent model turbine arrays when deployed in a similarly confined channel [13]. (There appears to be no fundamental difference in the wakes produced behind mesh discs and rotating turbines.). The single-rotor turbines used here introduced swirl into the wake, which was detectable by the ultrasonic probe traversing downstream.

The persistence of the wake threatens to ‘shadow’ any turbines placed further downstream. To demonstrate this in the negative sense, a 1+2 array (1 turbine upstream, 2 turbines side by side downstream) was tested with the turbines initially disposed over the cross-sectional area of the flume as shown in Figure 31. If there is any expansion of the wake behind the upstream turbine, those downstream will be affected.

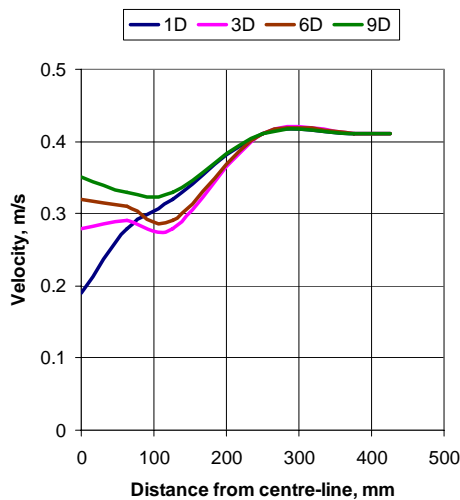


Figure 30: Velocity traverse in the wake of a single turbine, at various turbine diameters (D) downstream.

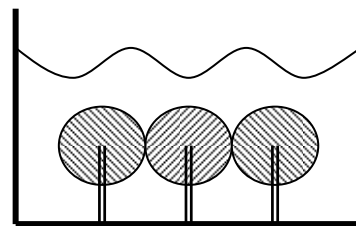


Figure 31: Location in test flume of model turbines in 1+2 array.

The single downstream turbine was tested in various positions along the centre-line of the flume: 3, 6 and 9 rotor diameters ahead of the downstream pair. Tests were then repeated with the turbine displaced laterally by 125 mm and 250 mm, in the latter case completely masking one of the downstream turbines. For each configuration, the power output of the downstream turbines was monitored. The results are shown in Figure 32; the output of a downstream turbine is expressed as a percentage of its nominal free stream value, with the legend at the top of the figure referring to the distance (in mm) by which the upstream turbine is displaced from the flume centre-line.

An interesting finding was that with the upstream turbine centrally located, its wake had no measurable effect on those downstream. A lateral displacement of 125 mm (half a rotor diameter) caused the output from the shadowed turbine to fall slightly, while full shadowing at 250 mm displacement reduced it further as expected, with the effects diminished as the spacing between upstream and downstream turbines was increased. There was no measurable recovery between 6 and 9 diameters of spacing for the fully masked turbine.

The configuration used here has a high blockage factor (37%), which might not be representative of real deployments. There is experimental evidence [13] that wake behaviour is particularly sensitive to the proximity of boundary walls. Free-stream turbulence is also likely to be a major factor: the test flume had turbulent intensities ranging from 10% to 25% at the working section, which might have been expected to cause rapid mixing between the wake and the surrounding stream, but there was little evidence that this occurred in the experiments.

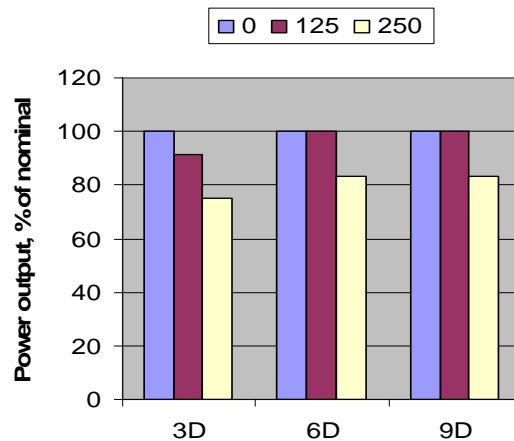


Figure 32: Effects of wake from a single turbine on the power output of a turbine placed downstream against various centre line offsets.

There is clearly scope for more work on wake development and array performance, using both computational and physical models. Critical issues to be resolved include:

- the effects of free-stream turbulence on wake dispersal;
- the importance of the degree of swirl and turbulence characteristics of the wake; and
- the effects of proximity to flow boundaries or other fixed objects.

At present it appears that the wakes behind marine current turbines persist for many rotor diameters downstream, having major implications for array design. The result could be that the sequential elements of large arrays will need to be placed much further apart than would otherwise be desirable. Array performance can be optimised by adjusting the electrical loading on individual turbines within the array or by adjusting the wake dispersal characteristics of the turbine as with CoRMaT.

Lessons learned from testing

Electrical

Permanent generator design

The axial flux generator worked well within the project although the concept of fully flooded operation clearly needs longer-term evaluation. The diameter of a direct drive generator (due to slow prime mover rotational speed) makes it difficult to produce a highly efficient tidal turbine form-factor, but this may be a price worth paying if it permits the elimination of the gearbox. Care must be taken when assembling and disassembling the 2 magnetic rotors of the generator due to the extremely strong nature of the magnets.

Brush and slip ring seal failure

The sealed brush and slip ring arrangement was designed and manufactured in-house. The arrangement proved to be reliable in terms of electrical contact. However, the double-ended sealing between the main shaft and slip ring housing proved problematic. Water ingress was observed during all test cases even when the cavity was packed with non-conducting (electrical) grease. The sealing arrangement was insufficient and major redesign with multiple spring actuated seals would be

necessary to cope with the external water pressure. The friction of multiple seals would however degrade the power performance of such a small scale device.

The large scale 250 kW prototype slip-rings have been designed in Canada by Moog/McCartney Ltd, leaders in sub-sea high-power transfer technology. They adapted an existing design for our purposes; however the design life of 5,000,000 revolutions would be the equivalent of 6 months of CoRMaT use, which is probably insufficient.

Instrumentation

Data logging

Data should be logged at a high frequency using a duplicated system for redundancy with a third telemetry method for backup. This may seem like overkill, however the cost of losing data through corruption, the device being lost, or the sampling frequency being found to be insufficient is considerably higher than implementing these measures. Capturing remote data from a tidal turbine is problematic. The option of a long cable link is possible and RS485 would be recommended, however this would depend on digitising, multiplexing and encoding at the turbine end. A long cable increases the risk of snagging and breakage in a seldom stationary marine environment. The other less problematic option is to digitise, multiplex, encode and wirelessly transmit data from a surface buoy (high frequency radio waves do not travel well through water). The latter was chosen and cheaply implemented in-house.

Data telemetry

While the wireless data stream sent to the St Hilda was invaluable to monitor and control turbine performance, it is not of a sufficiently high resolution or robustness (due to transmission and range errors) to be used in the final performance analysis. The solid state data recorder (Gigalogger) provides the best data set to undertake this on its 8 analogue channels and the full digital RS232 record of all data streams.

Micro-processor RPM delays

It is notable that due to the simple linear code implementation on the PIC microprocessor, when counting the digital pulse duration associated with the RPM and tidal velocity meter outputs, a delay is imposed on the data flow from all other sensors. For this reason a solid state data logger was also used to record high resolution data without this limitation.

Tidal velocity meter outages

During testing it was found that when the PWM was changed to provide turbine electrical loading the tidal velocity information became unreliable. Although the reason for this is unclear, it was possible to extrapolate between reliable readings to deduce the tidal velocity. Additionally, as the velocity impeller was solidly attached to the turbine, any turbine pitching affected the velocity reading. In future it would be appropriate to provide a gimbal system to maintain the tidal velocity meter at a constant angle into the tidal stream, or to locate the sensor elsewhere

RPM tachometer

Although optical and electrical contact tachometers are common they are not usually suitable for underwater immersed use. A set of magnets equidistantly spaced around the circular perimeter of the rotor stub are picked up by a single sealed magnetic reed switch. The accurate spacing of the magnets is critical to accurate RPM readings – this was achieved using a CNC mill.

Load cell force logging

The IP68 load cells utilised in earlier CoRMaT sea trials were adapted and utilised to measure the forces in the mooring line and turbine strut. While all equipment was of IP68 standard (long term immersion to a specified pressure), the IP68 cable connectors leaked at depths below 8 m. This was partly due to the depth and possibly the mechanical strain on the cables associated with drag forces in the tidal stream. One solution would be to use proper (expensive) subsea cable connectors. As the

force logging required extra datalogger channels, a second Gigalog was employed to acquire and store the load cell data. A channel from the original data logger (buoy inclinometer M_y) was also recorded in order to provide a consistent synchronous time base for measurement comparison.

Mechanical and Dynamics

Blade attachment

On retrieval at Islay, the bolts retaining a blade on the turbine were found to be loose. This was probably due to an under-tightened bolt after an onboard repair that subsequently worked itself loose in the turbulence of the tidal stream. A robust bolt locking mechanism and perhaps a damping mechanism would alleviate this problem, which would otherwise likely result in complete blade loss over any longer duration of operation. The alloy blades utilised on CoRMaT were modified versions of those from the initial tow-tank tests. This required the original blade stubs to be removed and new flat mounting flanges to be welded onto the blade root. Although a jig was used to do this, it is unlikely that all the blades remained exactly similar. Additionally, the alloy welding is prone to fatigue and stress cracks were observed post deployment. Any full scale version would not use similar alloy blades.

Turbine neutral buoyancy

Although turbine weight was carefully accounted for during design, a very small amount of miscalculation will lead to the turbine not being neutrally buoyant and therefore unable to maintain itself in stable horizontal position. The tail was thus deliberately made buoyant and a space left on the back end of the central spinal shaft for additional weights to be added and allow the proper horizontal trim to be achieved. This was particularly important as the tow-tank tests were in fresh water and the others in sea water - which have different densities and thus trim requirements. The addition of any marine fouling is likely to affect device trim over any period of time within the sea. During initial testing the air filled buoyancy chambers in the rear nacelle leaked – this was remedied for later tests by filling the void with closed cell expanding foam.

Central shaft – hollow bore

In order to pass power and instrumentation cables past the contra-rotating blades, a hollowed spinal shaft was utilised. This not only provided the main structural element onto which the rotors mounted but also the connection point for the mooring system. The shaft was sized based on the weight of the components in air, however due to increases in the design weight the shaft became slightly bent when in air. This was not a problem in sea-water where the weight is reduced. Additionally, the smallest bore of shaft possible was chosen, retaining sufficient strength while allowing a central hollowed-out section for the cables. This was selected in order to utilise the smallest outer shaft bore seals possible to reduce friction and also minimise water ingress. The practicalities of feeding the instrumentation and power cables into such a narrow space proved difficult and future hollow spinal shafts should have a significantly larger diameter bore for better access.

Dynamic instability due to turbine strut

FFT analysis displayed a large dynamic pitching moment that was found to be due to vortex shedding behind the vertical tubular section connecting the turbine to the surface buoy. This requires design modification.

Nacelle size

In order to accommodate the direct drive PMG a large nacelle diameter was required. In combination with the short alloy turbine blades, this produced instabilities and inefficiencies for the overall system.

Compliant mooring cable

A compliant cable from the seabed foundation, to the turbine, to the surface buoy was trialled at the Kyles of Bute. This arrangement was found to tangle very easily resulting in the turbine malfunctioning and loss of some of the foundation components (this was the only loss of equipment at sea during all of the testing). The mooring system was adapted for the Islay tests with the addition of a

rigid strut between the turbine and surface buoy. This was found to work well without any tangling, however wave action and dynamics would be a future design factor.

Compliant mooring material

Initially, a sheathed nylon braid mooring line was used, which proved to be bulky and became easily knotted, tangled and fouled. For the second series of tests, a braided stainless steel wire rope was used. Although more difficult to store and deploy without kinking, this proved to be a robust solution.

General

Sea testing in Scotland is highly dependent on the weather. Testing during the late spring or summer months is likely to prove most profitable. It is not the operation of the device or ability of the vessel to anchor on site, so much as being able to deploy and recover the device in anything other than fairly stable conditions. Experimental work involving equipment being deployed in hostile marine conditions requires extreme attention to detail if disaster is to be avoided. This particularly applies to waterproofing and the continuous checking of all load bearing components. Generally “what can go wrong, will go wrong”. To this end a full set of appropriate spares and tools should be carried as replacements are likely to be some (expensive) days away.

Site identification

At the Kyles of Bute a number of possible deployment sites were initially selected from a study of the nautical charts. The required depth (5-8 m), enough room to manoeuvre the tender vessel, good anchorage proximity to receive the radio telemetry, and being outwith shipping channels quickly narrowed down suitable deployment sites. The selection of the chosen position (55°55.393N, 005°10.026W) was determined by surface velocity measurements (using a modified Nortek Vectrino) and observation of the turbulence in the flow from a dinghy at different points in the tidal cycle.

The use of a ship-borne ADCP to take tidal velocity transects would be necessary to gain a better picture of subsea tidal flow over long periods before full deployment. Additionally, a ship-borne side scan sonar could be used to provide bathymetry data for any proposed site.

Foundation deployment and recovery

To avoid complexity and reduce installation time the system should ideally be deployed and retrieved as a single unit. Efforts to deploy and retrieve the foundations in sections proved very awkward even in the calmer waters of the Kyles of Bute.

Insurance and Risk Assessment

It was not possible to insure the device itself, however all other activities and personnel were covered by arrangement with the University’s insurers. This was dependent on a full risk assessment and a method statement for deployment and recovery of the CoRMaT system.

Sea versus tank testing

Although the testing at sea was significantly cheaper than tow-tank testing, it is impossible to replicate and control the sea environment in a repeatable manner. Tow-tank testing is therefore an invaluable tool despite its expense - in real terms every parameter is more readily measured and repeated, and an efficient day of tank testing can produce the equivalent evaluation of many tidal cycles at sea. That said, it is obvious that any proposed tidal system that has not been evaluated in the sea is unlikely to produce satisfactory confidence for investors, but the balance should initially be towards the controlled test-tank environment.

Scale of devices and handling vessel

The CorMaT device was at a very suitable size for launch and recovery from the tender vessel St Hilda. A HIAB such as those on the stern of trawlers would significantly have helped matters, particularly in terms of deploying and recovering the heavy concrete foundation.

Conclusions

A prototype contra-rotating marine current turbine has been constructed and laboratory testing and sea trials carried out on component parts and the complete system. Tests in a towing tank have demonstrated that a contra-rotating turbine with near-zero reactive torque on the support structure, near-zero swirl in the wake, and high relative inter-rotor rotational speeds can operate successfully. Power coefficients were encouragingly high and the excellent agreement with predicted values has established confidence in the novel aspects of the computational models used in the design procedure. High-frequency blade loading data were obtained from subsequent sea trials. These show the anticipated dynamic components for a contra-rotating machine. Finally, the complete system comprising contra-rotating rotors, contra-rotating, direct drive generator, and buoyancy chambers was tested under realistic deployment conditions.

References

1. Clarke J A, Connor G, Grant A D and Johnstone C M (2005) 'Design and initial laboratory testing of a contra-rotating tidal current turbine', *Proc 6th European Wave and Tidal Energy Conf.*, Glasgow.
2. Clarke, J A, Connor, G, Grant, A D and Johnstone, C M (2007) 'Design and sea testing of a contra-rotating tidal current turbine', *Journal of Power and Energy*, V221(2), pp171-179.
3. www.marineturbines.com (viewed 15 April 2009).
4. Myers L and Bahaj A J (2007) 'Wake studies of a 1/30th scale horizontal axis marine turbine', *Ocean Engineering*, V34, pp758-762.
5. Kim H W and Brown R E (2006) 'Coaxial rotor performance and wake dynamics in steady and manoeuvring flight', *Proc. American Helicopter Society 62nd Forum*, Phoenix.
6. McCombes T, Grant A and Johnstone C (2008) 'Wake modelling for marine current turbines', *Proc. 2nd Int. Conf. on Ocean Energy*, Brest.
7. Manwell J F, McGowan J G and Rogers A L (2002) 'Theory, Design and Application', Chapter 2 in *Wind Energy Explained*, Wiley, ISBN 0-471-49972-2.
8. Somers D M (1997) 'Design and experimental results for the S814 airfoil', *Subcontractor report NREL/SR-440-601*, Airfoil Incorporated, State College, Pennsylvania.
9. Barltrop N D P *et al* (2005) 'Wave-current interactions in marine current turbines', *Proc. of the 6th European Wave and Tidal Energy Conference*, Glasgow.
10. Soderlund L, Eriksson J T, Salonen J, Vihriala H and Perala R A (1996) 'Permanent-Magnet Generator for Wind Power Applications', *IEEE Transactions on Magnetics*, V32(4).
11. Segergren E, Nilsson K and Leijon M (2004) 'Frequency Optimisation with Respect to Weight and Electrical Efficiency for Direct Drive Underwater Power Generator', *Oceanic Engineering*.
12. Nilsson K, Segergren E, Sundberg J, Sjostedt E and Leijon M (2004) 'Converting Kinetic Energy in Small Watercourses Using Direct Drive Generators', *Proc. OMAE04 23rd Int. Conf. on Offshore Mechanics and Arctic Engineering*, Vancouver.
13. Myers L, Bahaj B, Germain G and Giles J (2008) 'Flow boundary interaction effects for marine current energy conversion', *Proc. 10th World Renewable Energy Congress*, Glasgow.